FIELD STUDY ON FRACTURE PROPAGATION IN WEAK SNOWPACK LAYERS

Alec van Herwijnen[1,*], Joachim Heierli[2,3] and Jürg Schweizer[1]
[1] WSL, Swiss Federal Institute for Snow and Avalanche Research SLF Davos, Switzerland
[2] Centre for Materials Science and Engineering, The University of Edinburgh, Scotland
[3] Institut für Zuverlässigkeit von Bauteilen und Systemen, Universität Karlsruhe, Germany

ABSTRACT: Instabilities in snow slopes generally involve the progressive fracture along a weak snowpack layer. Recent field observations on fractures in weak layers have shown that this process results vertical displacement due to crushing of the weak layer. Long beam specimens containing a natural weak layer were used to study the propagation of fracture. Multiple black markers were inserted in the snow above and below the weak layer. The deformation of the slab during fracture propagation was recorded with a portable digital high speed camera. A technique to reconstruct the trajectories of the markers was developed. This resulted in a detailed visualization of the deformation of the slab during fracture propagation. Results show the propagation of a wave through the slab associated with the collapse of the weak layer. Propagation velocities were relatively constant in the middle of the beam and increased towards the edges. The propagation speed in the middle of the beam was 20 ms^{-1}, in agreement with theoretical predictions of a new theory for fracture propagation in weak snowpack layers.

KEYWORDS: snow avalanche, avalanche release, fracture mechanics, fracture propagation

1. INTRODUCTION

In order for a snow slab avalanche to release, an initial failure in a weak layer has to propagate below the slab. For natural slab avalanches it is believed that the initial failure is caused by a gradual damage process at the micro scale leading to a localized failure within the weak layer. For artificially triggered avalanches (e.g. skier-triggered avalanches) the external trigger induces localized deformations which are large enough to initiate a failure within the weak layer. If the initial failure in the weak layer reaches a critical size it will propagate below the slab and usually results in the release of a slab avalanche (Schweizer et al., 2003).

The first direct measurement on fracture propagation through a weak snowpack layer was performed by Johnson et al. (2004). Using geophones placed on the snow surface on low angle terrain, a fracture speed of 20 ms^{-1} was measured. Further field observations of fractures in weak snowpack layers (Schweizer et al., 1995; van Herwijnen and Jamieson, 2005) have shown that fracturing of weak layers is accompanied by slope normal displacement (i.e. crushing of the weak layer). The crushing follows from the highly porous nature of these weak layers and of snow in general. Jamieson and Schweizer (2000) suggested that the release of potential energy during collapse might help to drive fracture propagation. Recently a new theory for fracture propagation by mixed mode anti-cracks has been proposed by Heierli et al. (2008). Crushing of the weak layer and the work of the compressive component of the stress field are taken into account.

Recently, field tests that focus on fracture propagation were developed (Gauthier and Jamieson, 2006; Sigrist and Schweizer, 2007). By cutting the weak layer in an isolated beam with a snow saw, the propagation propensity is evaluated.

For the current study, fractures in weak snowpack layers in three beam tests were recorded using a high speed camera. The aim was to obtain detailed displacement and velocity measurements at the time of fracture and to determine the propagation speed.

2. METHODS

2.1 Field methods

The high-speed camera (VDS Vosskühler HCC-1000) which was used has a resolution of 1024x512 effective pixels. Images were recorded at approximately 300 frames per second (fps), depending on aperture and shutter speed. The internal memory of the camera can store a sequence of up to 1024 images until a trigger is received. After each test the images were transferred to a portable computer.

Corresponding author address: Alec van Herwijnen, WSL Institute for Snow and Avalanche Research SLF, Flüelastrasse 11, 7260 Davos, Switzerland; tel: +41 81 4170175; fax: +41 81 4170110; email: vanherwijnen@slf.ch

Fractures propagating through weak snowpack layers were observed in beam tests. Snow beams containing a weak layer were isolated on all four sides from the surrounding snow down to a depth below the weak layer of interest (Figure 1a). The beams were 30 cm wide in the cross slope direction and 3 to 4 m long. Beginning at the down-slope edge of the beam, the weak layer was quickly cut using a 2 mm wide snow saw until the fracture started propagating (Figure 1b). The length of the saw cut through the weak layer at fracture propagation, i.e. the cut length r_c, was recorded.

In order to visualize the deformation of the slab during fracture propagation one side of the beam test was completely exposed by shovelling. Black markers were inserted in the snow above the weak layer in a regular grid pattern (Figure 1). Typically, the distance between the markers was 10 to 15 cm. Markers were also inserted in the snow below the weak layer. The camera was mounted horizontally on a tripod, aimed at the exposed side of the beam and the test was performed until the weak layer fractured. Propagating fractures were photographed in three beam tests on low angle slopes. The tested weak layers consisted of either buried surface hoar (SH) or faceted crystals (FC). In the first two tests, referred to as test A and B, there were two rows of markers in the slab. The third beam test, test C, had four rows of markers in the slab above the weak layer.

Additionally, at each test site, a snow profile was observed to obtain information about hand hardness, crystal type, crystal size, layer thickness, temperature and density of the snow layers (CAA, 2002).

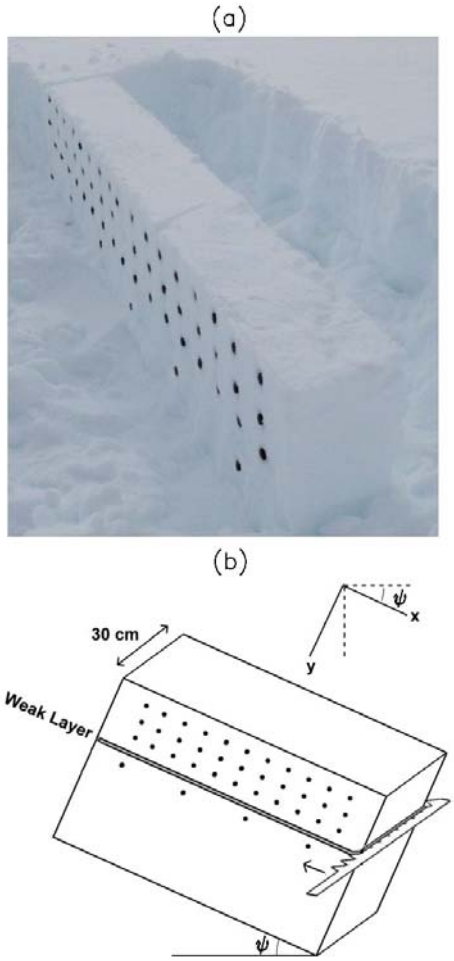

Figure 1: Propagating fractures in weak snowpack layers were photographed in long beam tests using a high speed camera. (a) Photo of an isolated beam with black markers in the snow. (b) Schematic representation of the test geometry and coordinate system used in the image analysis

2.2 Particle tracking and fracture speed calculation

Particle tracking software (Crocker and Grier, 1996) was used to analyse the images of propagating fractures. A spatial band pass filter is used to locate the markers by searching for a local brightness maximum and coordinates are assigned to the centroid of each marker. This was done for all the images in the sequence so that at any given time the position of all the markers was known. By 'connecting the dots' between subsequent images the trajectories of the markers were determined.

When analysing the images, a coordinate system with a slope parallel (x) and a slope normal (y) axes was used (Figure 1b). The displacement of a marker was calculated as the departure from its initial position:

$$\Delta x(t) = x(t) - x_0$$
$$\Delta y(t) = x(t) - y_0 \qquad (1)$$

where the initial position (x_0,y_0) was determined by averaging the position of the marker over 50 frames prior to movement. The final displacements in slope parallel and slope normal direction after fracture propagation are denoted by Δx_{max} and Δy_{max}, respectively.

The velocity of a marker (v_x,v_y) was calculated from the displacements:

$$v_x(t) = \frac{\Delta x(t) - \Delta x(t-\Delta t)}{\Delta t} \qquad (2)$$
$$v_y(t) = \frac{\Delta y(t) - \Delta y(t-\Delta t)}{\Delta t}$$

where Δt is the time between two subsequent frames (i.e. 1/300 s).

For propagating fractures there is a delay between the slope normal displacement of subsequent markers. The time delay between the onset of movement between two markers is proportional to the distance between the markers and directly relates to the propagation speed *c* of the fracture front (van Herwijnen and Jamieson, 2005).

The accuracy of the particle tracking software depends on the size and the quality of the images, i.e. signal-to-noise ratio. The choice of the magnification is a trade-off between the size of the field of view (FOV) and the degree of image contrast and the apparent particle size, i.e. the size of the markers in the digital images. For this study, the particle radius was typically 10 pixels corresponding to a magnification of 3 mm/pixel and a field of view of approximately 3 m. For each test, the accuracy ε was determined by calculating the standard deviation in the initial position of the markers. The accuracy was on the order of 0.2 mm.

2.3 Refinement of trajectories

The particle tracking software easily attains an accuracy better than 1/10 pixel even with moderate signal-to-noise ratio (Crocker and Grier, 1996). However, uneven pixel clipping at the edges of the markers introduced some scatter in the displacement data. Pixel clipping occurs when the edge of a marker is located between two pixels on the digital image, causing scatter in the location estimation. This can occur when a particle is stationary, termed static pixel clipping, or when the particle is in motion, termed dynamic pixel clipping

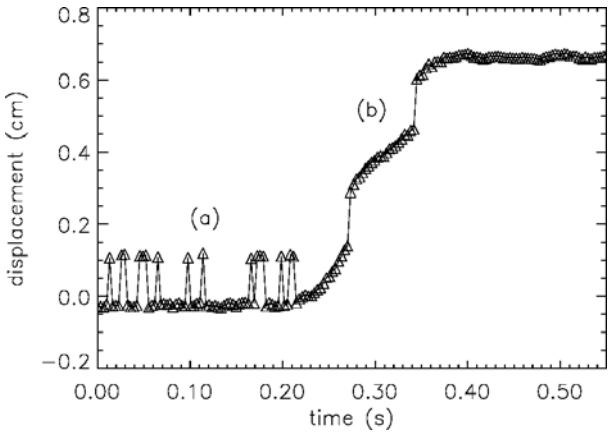

Figure 2: Example of the trajectory of a marker with static (a) and dynamic (b) pixel clipping . The triangles represent the centroid of the marker in each frame

(Figure 2). Pixel clipping only occurred for markers which were located on sections of the beam where there was uneven illumination.

In order to eliminate this unwanted effect a method was developed to correct for uneven pixel clipping. The method is based on the fact that a jump in the displacement corresponds to a sharp peak in the velocity of the marker, much larger than the velocity of the marker caused by the actual movement. These peaks were identified by choosing a suitable threshold value for the marker velocity data. Points that fell above this threshold, were assigned a new value corresponding to the average marker speed of the two closest data points which were below the threshold value. The refined trajectory was obtained by integrating the smoothed and corrected marker velocity.

3. RESULTS

Three propagating fractures were photographed in beam tests with black markers in the snow wall above the weak layer (Table 1). Tests A

Table 1: Measurements from photographed fractures in beam tests. Slope angle (φ), field of view of the camera (FOV), frame rate of the recording (fps), accuracy of the displacement measurements (ε), weak layer crystal type (*F*), depth of the weak layer measured vertically (*H*), weak layer thickness measured vertically (*h*), average slab density (ρ_{slab}), cut length at fracture propagation (r_c). The maximum slope parallel and slope normal displacement, Δx_{max} and Δy_{max} respectively, and the fracture propagation speed (*c*) were derived from the refined trajectories.

Test	φ (°)	FOV (cm)	fps	ε (cm)	*F*	*H* (cm)	*h* (cm)	ρ_{slab} (kg m^{-3})	r_c	Δx_{max} (cm)	Δy_{max} (cm)	*c* (m s^{-1})
A	11	305	307.92	0.02	SH	38	3	300	16	1.48-1.96	2.36-4.07	32±2
B	11	305	307.92	0.02	SH	38	3	300	19	1.39-1.64	2.75-3.47	35±2
C	19	280	307.33	0.01	FC	43	9	250	44	0.20-0.35	0.52-0.83	27±1

and B were performed on a layer of large buried surface hoar crystals (30 to 40 mm) and with two rows of markers inserted in the slab. Preliminary beam tests on this layer, which was buried 20 cm below the surface, did not result in full propagation of the fracture through the weak layer even though we had whumpf on this layer the day before. Therefore, we increased the load above the weak layer by shovelling additional snow on top of the existing slab. We waited a few hours for the snow to settle before performing more beam tests. With the additional load, the fracture propagated through the whole length of the beam. In both tests we observed vertical fractures through the slab roughly halfway through the beam. Test C was performed on a layer of facetted crystals (1.5 to 2.5 mm) underlying a thin crust. The fracture propagated through the entire beam and no vertical fractures were observed through the slab.

3.1 Displacement of markers

The total displacement of the markers, in both the slope parallel and slope normal direction, was not the same for all markers (range given in Table 1). The slope normal displacement generally decreased with increasing distance from the down-slope edge of the beam, where the fracture was initiated, in all three tests. Such a trend was not observed in the slope parallel displacement. Furthermore, for each marker the total slope normal displacement was always larger than the total slope parallel displacement (Table 1).

In Figure 3 the displacements of all the markers in Test C are shown at the onset of fracture propagation, during fracture propagation,

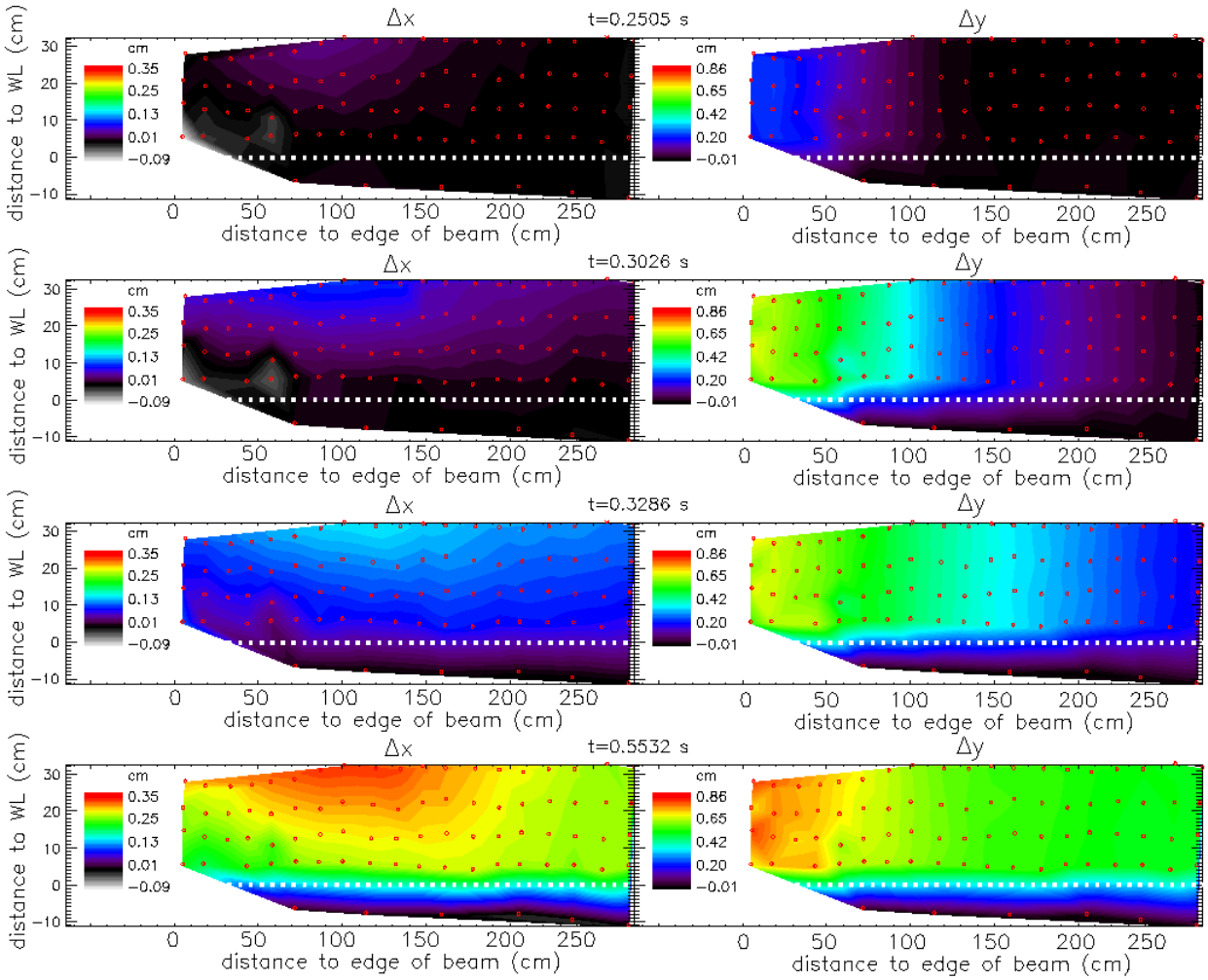

Figure 3: Slope parallel (Δ*x*, left) and slope normal (Δ*y*, right) displacement for a fracture propagating through a weak layer composed of faceted crystals (test C). Displacements are shown at the onset of fracture propagation (*t* = 0.2505 s), during fracture propagation (*t* = 0.3026 s), when the fracture reached the end of the beam (*t* = 0.3286 s) and at the end of the recording (*t* = 0.5532 s). The dashed white line indicates the weak layer and the red dots indicate the initial position of the markers.

when the fracture reached the end of the beam and at the end of the video recording. There was a clear difference in the behaviour of the slope parallel and slope normal displacement.

At the start of propagation (t = 0.2505 s) the slope normal displacement was largest in the first 50 cm of the beam, where the fracture was initiated, decreasing to zero at approximately 110 cm. As the fracture advanced through the beam and up to the end of the experiment, Δy remained largest at the edge of the beam gradually decreasing further away (right side Figure 3). Furthermore, there was no clear difference in Δy for markers close to the weak layer and those higher up in the slab, closer to the snow surface.

The slope parallel displacement was concentrated in the upper half of the beam, i.e. close to the snow surface. At the onset of fracture propagation (t = 0.2505 s) and during fracture propagation (t = 0.3026 s) Δx was largest in the row of markers closest to the snow surface, peaking at 100 to 150 cm from the edge of the beam while the row of markers closest to the weak layer was not displaced. At t = 0.3286 s, when the fracture reached the end of the beam, and at the end of the experiment (t = 0.5532 s), the same picture emerged. However, the row of markers closest to the weak layer was also displaced and the largest Δx was observed closest to the snow surface between 50 and 150 cm from the edge of the beam. Finally, during the entire test there was no discernable displacement of the markers below the weak layer.

3.2 Velocity of markers

In Figure 4 the velocity of all markers in test C at three different times, corresponding to the first three images in Figure 3, is shown. Again there was a clear distinction in the behaviour of the slope parallel and slope normal velocity of the markers.

At the onset of fracture propagation (t = 0.2505 s) v_y was largest at the edge of the beam, decreasing to zero at approximately 150 cm (top right in Figure 4), similar to the slope normal displacement (top right in Figure 3). As the fracture propagated through the beam (t = 0.3026 s) v_y became very small at the edge of the beam,

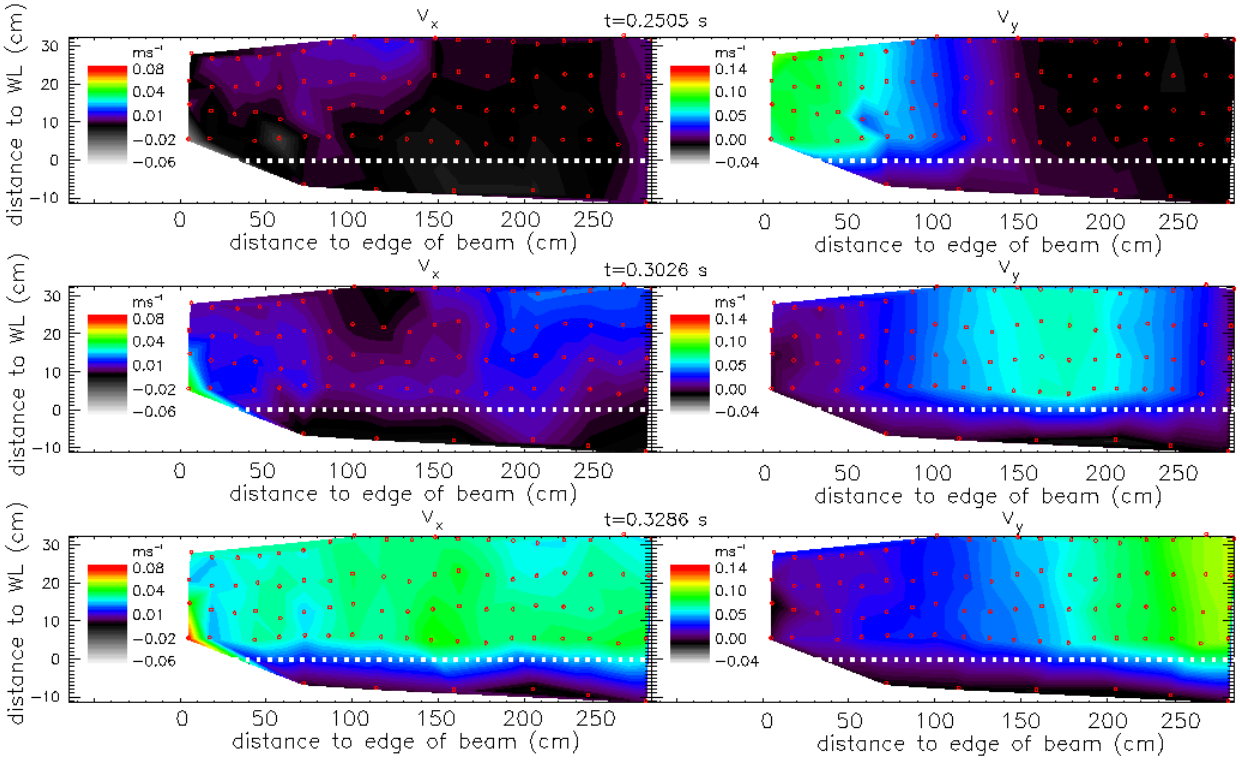

Figure 4: Slope parallel (v_x, left) and slope normal (v_y, right) velocity of the markers for a fracture propagating through a weak layer composed of faceted crystals (test C). Speeds are shown at the onset of fracture propagation (t = 0.2505 s), during fracture propagation (t = 0.3026 s) and when the fracture reached the end of the beam (t = 0.3286 s). The dashed white line indicates the weak layer and the red dots indicate the initial position of the markers.

increased to a maximum at around 170 cm and dropped sharply to zero again at the end of the beam. At $t = 0.3286$ s, v_y gradually increased through the beam to reach a maximum at the end of the beam. The slope parallel velocity (left in Figure 4) was mostly zero at the onset of fracture, except in the upper half of the beam up to roughly 140 cm from the edge of the beam. On the contrary, during fracture propagation v_x was positive throughout the beam, except for an area close to the snow surface between 100 and 150 cm from the edge of the beam. Finally, when the fracture reached the end of the beam, v_x was roughly equal for all markers throughout the slab and much larger than before.

3.3 Fracture speed

The propagation speeds shown in Table 1 were calculated using the onset time of the slope normal displacement of rows of markers spanning the entire width of the beam. As such, these can be considered an average fracture speed through the beam. The calculated fracture speed for test A and B, in which there was a relatively large slope normal displacement, was somewhat higher than that in test C (Table 1).

In order to determine whether the propagation was stationary or accelerated, fracture speeds were determined for sections of the beams by only considering five subsequent markers for the calculation, corresponding to 50 to 75 cm long sections of the beam. In this way we essentially determined a moving average of the fracture speed throughout the beam. In test A, a vertical fracture through the slab divided the beam in two parts, a section of 160 cm (15 markers) and a section of 130 cm (13 markers). In test B the beam was split up in three sections, due to two vertical fractures, with a length of 180 cm (17 markers), 85 cm (8 markers) and 35 cm (3 markers), respectively. Since these vertical fractures through the slab disrupted the displacement of the markers, it is likely that these fractures also influenced the propagation of the fracture. Therefore, each section of the beam in test A and B, separated by the vertical fractures through the slab, where considered separately. The last section of the slab in test B only comprised three markers and was therefore not included.

In Figure 5 the calculated propagation speed c for all three tests is shown as function of the distance to the edge of the beam where the fracture in the weak layer was initiated. The propagation speeds in both tests A and B, which were performed on the same weak layer and on the same day, showed good accordance (Figure 5a). The propagation speed in the first section of the beam was larger than in the second section of the beam. It decreased from around 60 ms^{-1} at the edge of the beam to 32 ms^{-1} at 200 cm in the first section. In the second section, c initially decreased to a minimum of roughly 20 ms^{-1} at 280 cm after which it increased again.

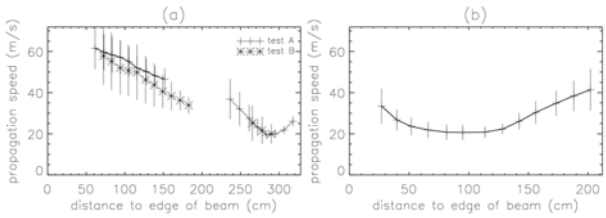

Figure 5: Fracture speed measurements as function of distance to the edge of the beam where the fracture was initiated. (a) results for test A (+ sign and solid line) and B (* sign and dashed line). (b) results for test C.

In test C the propagation speed decreased from 33 ms^{-1} at the edge of the beam to a relatively constant value of around 20 ms^{-1} between 60 and 130 cm. Thereafter the propagation speed increased and reached a maximum of 41 ms^{-1} at the end of the beam.

4. DISCUSSION

Beam tests were performed on low angle slopes to study fracture propagation through weak snowpack layers. On steeper slopes, the snow beam generally slides down-slope after the fracture has propagated through the weak layer. This results in additional slope parallel displacement which obscures the part of the displacement caused by weak layer fracturing. Therefore we decided to perform these tests on low angle slopes, where the beam did not slide down-slope after fracture propagation.

High-speed photography of fractures in weak snowpack showed experimentally that there is a compressive component associated with the fracture. Schweizer et al. (1995) reported slope normal displacement of 0.47 cm. Field measurements at whumpf sites, i.e. fracture propagation on low angle terrain, showed vertical displacements ranging from 0.08 to 1.0 cm (Johnson, 2000). Van Herwijnen and Jamieson (2005) measured slope normal displacements which ranged from 0.15 to 1.7 cm. These published values are comparable to the measured values in test C (Table 1). On the other hand, test A and B had larger slope normal displacements due to an unusually thick layer of buried surface

hoar crystals which was artificially loaded to achieve fracture propagation. Nevertheless, crushing of the weak layer has so far always been observed in all documented fractures through weak snowpack layers. It is a rule rather than an exception, which is not surprising given the highly porous nature of snow layers.

The total amount of slope normal displacement decreased with increasing distance from the edge of the beam where the fracture was initiated (Figure 3). One could argue that this is caused by the influence of the initial saw cut through the weak layer, which creates an artificial gap. However, results from test A and B showed that that the slope normal displacement was also larger behind vertical fractures through the slab (not shown). This suggests that the additional slope normal displacement is a boundary effect due to an unsupported edge of the beam and not caused by the saw cut. The edge of the beam where the fracture is initiated is unsupported. This allows the slab to move more freely resulting in more slope normal displacement. On the other hand, the slope normal displacement at the end of the beam, which is also an unsupported edge of the beam, was usually the smallest. This is likely due to the fact that the propagating collapsing fracture through the weak layer is abruptly stopped as it reaches the end of the beam, thereby disrupting the fracture process. Additionally, the velocity of the markers was also largest at both unsupported edges of the beam (Figure 4), highlighting the boundary effects due to the test geometry. In order to achieve stationary fracture propagation which is not influenced by boundary effects the beam should therefore be made longer than in our experiments.

The results depicted in Figure 3 show that the slope normal displacement preceded the slope parallel displacement, especially closer to the weak layer. This shows that when a weak layer fractures it collapses, likely due to rearrangement of the crystals in the weak layer, causing slope normal displacement. The slope parallel displacement is merely a secondary effect of the fracture process caused by the bending of the slab. When the weak layer collapses the slab undoubtedly bends, causing slope parallel displacement which increases closer to the snow surface (Figure 6). This is consistent with the results shown in Figure 3. During fracture propagation the onset of the slope normal displacement occurred simultaneously for markers close to the weak layer and those close to the snow surface. On the other hand, the slope parallel displacement was larger closer to the snow surface and preceded the slope parallel displacement closer to the weak layer (Figure 3).

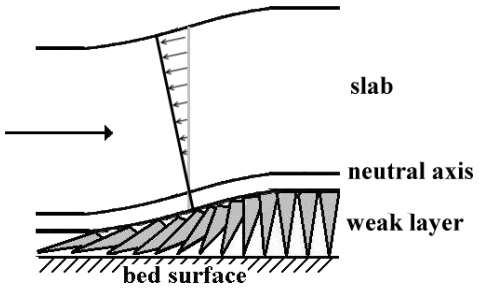

Figure 6: Schematic representation of bending of the slab associated with a propagating collapsing fracture through a weak snowpack layer.

The present results indicate that a recent new theory considering the collapse of the weak layer during fracture (Heierli et al., 2008) is more realistic to describe fracture propagation through weak snowpack layers than theories that only consider the slope parallel component of gravity as driving force for fracture propagation. The measured velocity of the markers during fracture propagation (Figure 4) showed that there was a wave propagating through the slab associated with the slope normal displacement, while this was not the case for the slope parallel displacement. This is in good qualitative agreement with the new theory.

The measured propagation speed values shown in Table 1 are slightly higher but in good agreement with other measured values which ranged from 17 to 26 ms^{-1} (Johnson et al., 2004; van Herwijnen and Jamieson, 2005). Furthermore, we were able to determine that the fractures in the beam tests were not stationary. In general, the propagation speed decreased from the edge of the beam where the fracture was initiated and increased again towards the end of the beam (Figure 5). Once again, this shows the influence of the unsupported edges of the beam on the fracture process. While the fracture in tests A and B propagated through the entire beam, the vertical fractures through the slab disturbed the fracture process. The propagation speed in these tests was rather high in the first section of the beam, decreasing to a minimum of around 20 ms^{-1} in the middle of the second section of the beam (Figure 5). Since these beams were artificially loaded, these measurements should be considered cautiously. On the other hand, in test C the fracture speed quickly attained a relatively stationary value of 20 ms^{-1} in the middle section of the beam. Since this is the part of the beam which is the least influenced by the boundaries of the beam we

consider these measurements most reliable. The theoretical prediction for the propagation speed in this experiment is 21 ms^{-1} (Heierli et al., 2008), in agreement with the measured values in the middle of the beam.

5. CONCLUSIONS

A portable digital high-speed camera was used to observe in-situ fractures in weak snowpack layers. Particle tracking software was used to track the displacement of multiple markers in the snow above the weak layer and an efficient signal processing method was developed to remove the effects of pixel clipping which was present in some trajectories. This resulted in a detailed visualization of the deformation of the slab associated with the propagation of a fracture through a weak layer and provided new insight into fracture propagation through a weak snowpack layer. Slope normal displacement, which ranged from 0.52 to 4.07 cm, was observed in all fractures and comparable to previously published measurements. Thus far, crushing of the weak layer has always been observed in all documented fractures through weak snowpack layers showing that this is inherent to the fracture process.

High accuracy displacement measurements showed the propagation of a wave through the slab associated with the collapse of the weak layer. The initial displacement of the slab was in the slope normal direction, due to crushing of the weak layer, and the slope parallel displacement was a result of the bending of the slab. This is in good qualitative agreement with a new theory for fracture propagation in weak snowpack layers (Heierli et al., 2008).

The results also showed the influence of the test geometry on the displacement and the propagation of the collapse wave. The displacement was influenced by the free boundaries of the beam in that it was largest at the edge of the beam where the fracture was initiated and smallest at the end of the beam where the propagation abruptly stopped. Furthermore, marker velocity was highest at both unsupported edges of the beam. In order to achieve stationary propagation, the beam tests should therefore be several meters long.

Propagation speed measurements using all markers throughout the slab ranged from 27 to 35 ms^{-1}, somewhat higher than previously published values. However, the results from two tests in which the weak layer was artificially loaded to achieve fracture propagation should be considered cautiously. Furthermore, it was shown that the propagating wave through the slab was not stationary throughout the beam. In one beam test the fracture speed quickly attained a relatively stationary value of 20 ms^{-1} in the middle section of the beam. This value corresponded very well to theoretical predictions as well as previously published results.

ACKNOWLEDGEMENTS

For their help with the field work, we would like to thank Sascha Bellaire and Christoph Mitterer. We gratefully acknowledge financial support by the European Commission under contract NEST-2005-PATH-COM-043386 (FP6, TRIGS) and DFG project Gu367/30.

REFERENCES

CAA, 2002: *Observation guidelines and recording standards for weather, snowpack and avalanches*. Canadian Avalanche Association (CAA), 78 pp.

Crocker, J.C. and D.G. Grier, 1996: Methods of digital video microscopy for colloidal studies. J. Colloid Interface Sci., 179 (1), 298-310.

Gauthier, D. and J.B. Jamieson, 2006: Towards a field test for fracture propagation propensity in weak snowpack layers. *J. Glaciol.*, **52**(176), 164-168.

Gauthier, D. and B. Jamieson, 2008: Evaluation of a prototype field test for fracture and failure propagation propensity in weak snowpack layers. *Cold Reg. Sci. Technol*, **51**(2-3), 87-97.

Heierli, J., A. van Herwijnen, P. Gumbsch and M. Zaiser, 2008: Anticracks: A new theory of fracture initiation and fracture propagation in snow. Proceedings ISSW 2008, International Snow Science Workshop, Whistler, Canada, 21-27 September 2008.

Jamieson, J. B. and J. Schweizer, 2000: Texture and strength changes of buried surface hoar layers with implications for dry snow-slab avalanche release. *J. Glaciol.*, **46**(152), 151-160.

Johnson, B., 2000: Remotely triggered slab avalanches. MSc. Thesis, University of Calgary, Calgary, Canada, 98 pp.

Johnson, B.C., B. Jamieson and R. Stewart, 2004: Seismic measurement of fracture speed in a weak snowpack layer. *Cold Reg. Sci. Technol*., **40** (1-2), 41-45.

Schweizer, J., J.B. Jamieson, and M. Schneebeli, 2003: Snow avalanche formation. *Rev. Geophys.*, **41**(4), 1016.

Schweizer, J., M. Schneebeli, C. Fierz, and P.M.B. Föhn, 1995: Snow mechanics and avalanche formation: Field experiments on the dynamic response of the snow cover. *Surv. Geophys.*, **16**(5-6), 621-633.

Sigrist, C. and J. Schweizer, 2007: Critical energy release rates of weak snowpack layers determined in field experiments. *Geophys. Res. Lett.*, **34**(3), L03502.

van Herwijnen, A. and B. Jamieson, 2005: High-speed photography of fractures in weak snowpack layers. Cold Reg. Sci. Technol., **43**(1-2), 71-82.